Journal of Alloys and Compounds 509 (2011) 9441–9446

Contents lists available at ScienceDirect

Journal of Alloys and Compounds

journal homepage: www.elsevier.com/locate/jallcom

Notch toughness of Fe-based bulk metallic glass and composites

S.F. Guo [a,b,c,*], K.C. Chan [b], L. Liu [a,**]

[a] State Key Lab for Materials Processing and Die & Mould Technology, Huazhong University of Science and Technology, 430074 Wuhan, China
[b] Advanced Manufacturing Technology Research Centre, Department of Industrial and Systems Engineering, The Hong Kong Polytechnic University, Hong Kong, China
[c] School of Materials Science and Engineering, Southwest University, 400715 Chongqing, China

ARTICLE INFO

Article history:
Received 15 February 2011
Received in revised form 7 July 2011
Accepted 8 July 2011
Available online 26 July 2011

Keywords:
Amorphous materials
Rapid-solidification
Quenching
Mechanical properties
Microstructure

ABSTRACT

The notch fracture toughness of $Fe_{75}Mo_5P_{10}C_{8.3}B_{1.7}$ monolithic bulk metallic glass (BMG) and $Fe_{77}Mo_5P_9C_{7.5}B_{1.5}$ and $Fe_{79}Mo_5P_8C_{6.7}B_{1.3}$ BMG matrix composites with α-Fe as reinforcing phase, fabricated by suction mould casting, were evaluated. It was found that the monolithic BMG has a toughness of 27 MPa $m^{1/2}$, while the $Fe_{77}Mo_5P_9C_{7.5}B_{1.5}$ BMG composite reinforced by single α-Fe dendrite phase exhibits a higher toughness of nearly 40 MPa $m^{1/2}$. However, for the $Fe_{79}Mo_5P_8C_{6.7}B_{1.3}$ alloy with more dendrites, the toughness decreased up to 25 MPa $m^{1/2}$. Microstructure investigation reveals that the simultaneous formation of Fe–Mo–P hard brittle phase apart from α-Fe dendrites in the $Fe_{79}Mo_5P_8C_{6.7}B_{1.3}$ alloy is the reason for the degradation of the fracture toughness.

1. Introduction

Uniaxial compression tests are widely used to evaluate the mechanical properties of bulk metallic glasses (BMGs) because all the monolithic BMGs look similar (zero ductility) under the tensile loading at ambient temperature with standard strain rate [1]. However, the data obtained from the conventional compression tests are not always reliable because the results are significantly affected by the sample geometry, confinement and machine stiffness effects [2,3]. In this regard, three-point-bending test is an alternate way to compare the mechanical properties of the different BMGs, especially their fracture toughness, which is a more useful parameter for practical significance in structural applications and reported currently in various BMGs [4–7].

Among the BMG family, Fe-based BMGs are of great interest due to their ultrahigh strength, excellent corrosion resistance and relatively low material cost [8,9]. Unfortunately, most of the Fe-based BMGs fail with extreme brittleness and exhibit very low fracture toughness, which limit their application as structure materials. How to improve the toughness of the Fe-based BMGs is the focus of the present research [10,11].

More recently, we have successfully developed an in situ α-Fe dendrites reinforced Fe-based BMG matrix composite with large compressive plasticity [12]. In this work, we provide a further investigation into the notch toughness of the Fe-based BMG and its matrix composites under three-point-bending mode. The mechanism of enhanced toughness will be discussed based on the fracture morphology observation.

2. Experimental

Multi-component master alloys with the compositions of $Fe_{75}Mo_5P_{10}C_{8.3}B_{1.7}$, $Fe_{77}Mo_5P_9C_{7.5}B_{1.5}$ and $Fe_{79}Mo_5P_8C_{6.7}B_{1.3}$ were prepared by arc melting of raw materials under a titanium metal gettered argon atmosphere [12]. Hereafter, the alloys are labeled as S20, S18 and S16, referring to the metalloids content of 20, 18 and 16 at.%, respectively. Sample rods with a diameter of 1.5 mm and a length of 50 mm were produced by suck casting method. The structure of the as-cast alloys was examined by X-ray diffraction (XRD), scanning electron microscopy (SEM) and transmission electron microscopy (TEM), respectively. The thermal properties of the alloys were investigated with a differential scanning calorimeter (DSC) under argon atmosphere at a heating rate of 0.33 K/s.

Samples for notch toughness measurements were taken from the as-cast rods with 1.5 mm diameter. Notches were made to a depth of approximately half of the rod using a slow-speed diamond saw. Three-point single edge notched bend tests fixture with span distance of 12 mm were performed on a Zwick/Roell testing machine under displacement control at 0.1 mm/min. About 10 samples were conducted for each composition to ensure the results reproducibility. Note that the notch toughness (K_Q, not K_{IC}) values were calculated by using standard references for this geometry [13].

3. Results and discussion

Fig. 1(a)–(d) shows the XRD patterns and the cross-section micrographs of the three as-cast alloys. It can be observed that the

* Corresponding author at: The State Key Lab of Materials Processing and Die & Mould Technology, Huazhong University of Science and Technology, China.
** Corresponding author.
E-mail addresses: sfguo2005@163.com (S.F. Guo), lliu2000@mail.hust.edu.cn (L. Liu).

0925-8388/$ – see front matter © 2011 Elsevier B.V. All rights reserved.
doi:10.1016/j.jallcom.2011.07.016

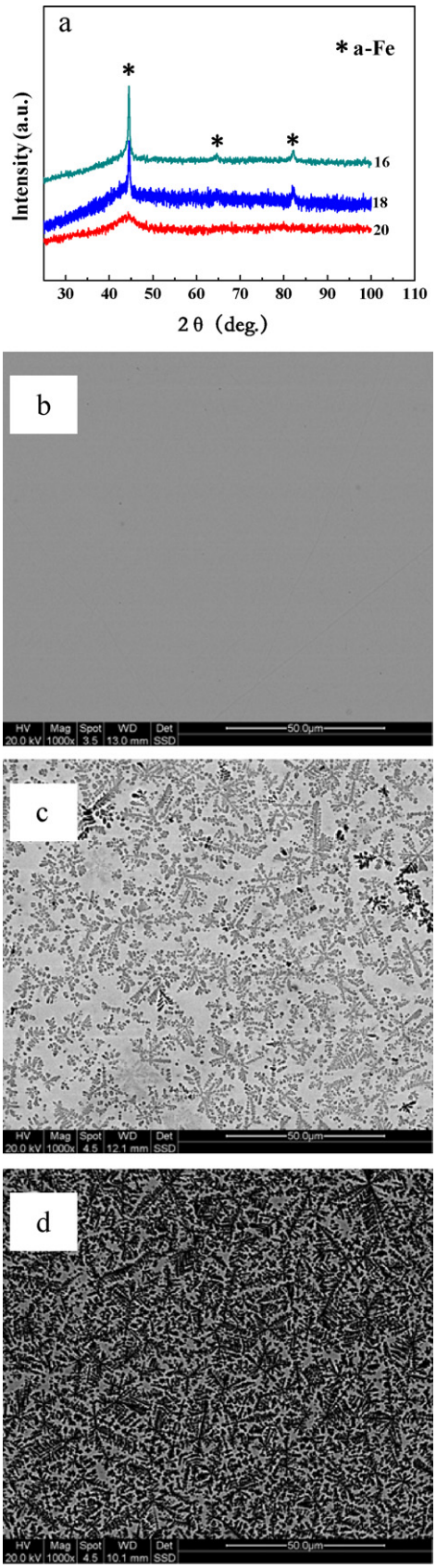

Fig. 1. (a) The XRD patterns of the as-cast S20, S18 and S16 alloys rod with a diameter of 1.5 mm and the corresponding SEM backscattered electron images of these three alloys (b), (c) and (d), respectively.

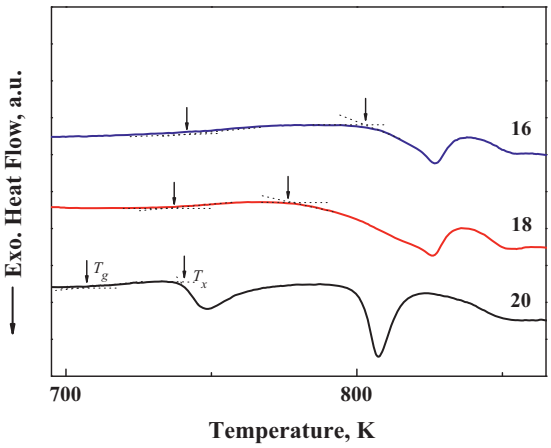

Fig. 2. The DSC scans recorded for S20, S18 and S16 alloys, respectively.

S20 sample exhibits only a broad halo diffraction peak in XRD pattern and featureless appearance in SEM image (Fig. 1(b)), indicating a fully amorphous structure of the alloy. However, for the alloys S18 and S16, a mixed structure of amorphous matrix together with bcc α-Fe dendrites was formed, demonstrating in situ synthesis of Fe-based BMG matrix composites (approximately 40% and 60% of volume fractions according to the area analysis from the SEM micrographs shown in Fig. 1(c) and (d), respectively).

Fig. 2 shows the DSC curves of the three alloys. It can be clearly seen that the alloy S20 with monotonic glassy structure exhibits a distinct glass transition with a relatively low glass transition temperature T_g (about 708 K) followed by two crystallization peaks with the onset temperature T_x of 740 K. However, for S18 and S16 BMG composites, the T_g increases up to 738 and 740 K, while the onset of crystallization temperature increase up to 776 and 803 K, respectively. The changes in T_g implies the change of composition of the residual glassy phase in S16 and S18 alloys. In additions, the first crystallization peak of S18 and S16 BMG composites completely disappeared, which is related to the precipitation of α-Fe phase in these two alloys.

Fig. 3(a) shows the appearance of the notched sample with the root diameter of about 250 μm for three-point bending test. Fig. 3(b) exhibits a plot of notch toughness K_Q vs. Fe contents for the three alloys. The monolithic BMG, i.e. the alloy of S20, has a toughness of 27 MPa $m^{1/2}$, which is actually higher than some brittle Fe-based BMGs (usually less than 10 MPa $m^{1/2}$) [14]. This can be attributed to the low glass transition temperature of the alloy, which is usually related to a low activation barrier for shear flow [15]. On the other hand, the composite alloy of S18 which has about 40% volume fraction of α-Fe dendrites exhibits a toughness of nearly 40 MPa $m^{1/2}$, indicating that precipitation of α-Fe dendrites could significantly enhance toughness. This value can be comparable to some tough Cu-based BMGs reported previously [5]. However, with a further increase in the dendrite phase, the toughness decreased to 25 MPa $m^{1/2}$ for the S16 alloy. To be noted that the large error bar for the toughness value originates from the possible existence of defects (such as voids) in samples induced in the suck casting process.

The fracture morphology of the alloys is an important basis for understanding their fracture toughness. Fig. 4(a) shows the SEM micrographs of the fracture surface for the S20 BMG. It can be seen that the fracture surface can be divided distinctly into the crack initiation zone just near the root (indicated by A) and instantaneous fracture zone (indicated by B). Fig. 4(b) and (c) are the amplified pictures from zone A and B, respectively. The mirror zone in the crack initiation exhibits the nanoscale periodic characterizes, which is always shown in some brittle BMGs. However, the ratio of mir-

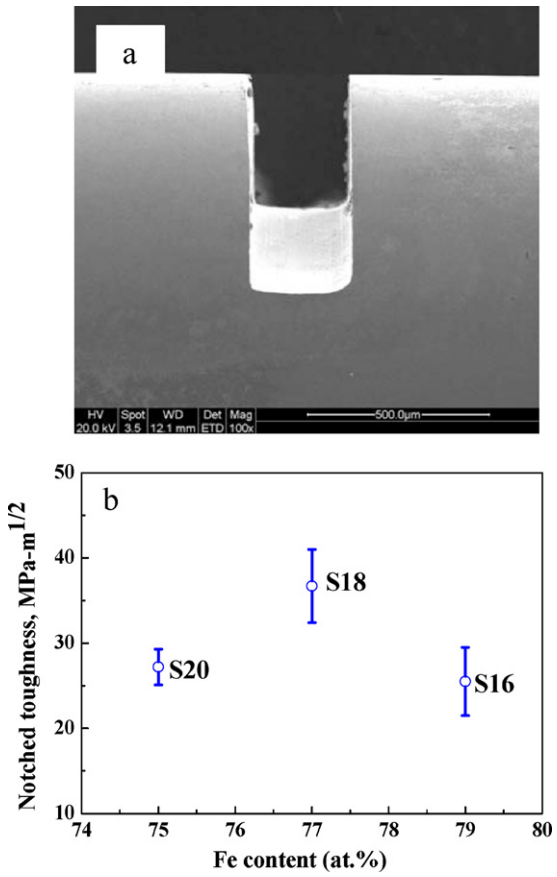

Fig. 3. The SEM image of preload S18 alloy (a) and the notch toughness vs. Fe content (b).

ror zone to the whole fracture surface for the present alloy is far less than those brittle BMGs reported [16,17]. In additions, using the equation of $w \approx 1/6\pi(K_C/\sigma_Y)^2$, the average critical plastic zone size w is estimated to be 6.3 μm, which is much larger than the wavelength of the initial perturbation of the meniscus (usually at nano-scale in brittle BMGs) proposed by Wang et al. [18]. Accordingly, the dimple-like patterns appeared at instantaneous fracture zone (see Fig. 4(c)) indicates that this Fe-based BMG is pretty tough at micro-scale.

Fig. 5(a) displays the SEM micrographs for the fractured surface of S18 alloy, which shows the highest toughness among the three alloys studied. In contrast to the monotonic BMG (S20), the fracture surface exhibits very rough characteristic without the mirror zone related to the crack initiation, but quite similar to the tough Zr-based BMG reported previously [4]. This is probably due to the strong interactions between cracks and soft α-Fe phase in the hard BMG matrix. Consequently, the cracks bifurcate and blunt in the crack initiation zone as shown in Fig. 5(b). This can be regard as one of energy dissipation mechanism and avoid the unstable crack propagation, resulting higher fracture toughness. In addition, when the crack further propagates to the instable stage (overload region), shallow dimples-like pattern was formed as shown in Fig. 5(c), which is typical feature for the instable propagation of cracks for BMGs.

Fig. 6(a) shows the SEM fractographs of S16 alloy with more α-Fe dendrites. Similar to the S18 alloy, the fracture surface of the alloy displays rough morphology. However, as shown in Fig. 6(b), it was found that some dendrites tear in the crack initiation zone and some voids were formed, implying that the fracture characterizes of this alloy looks like an intergranular fracture mode, i.e. sugar-like three

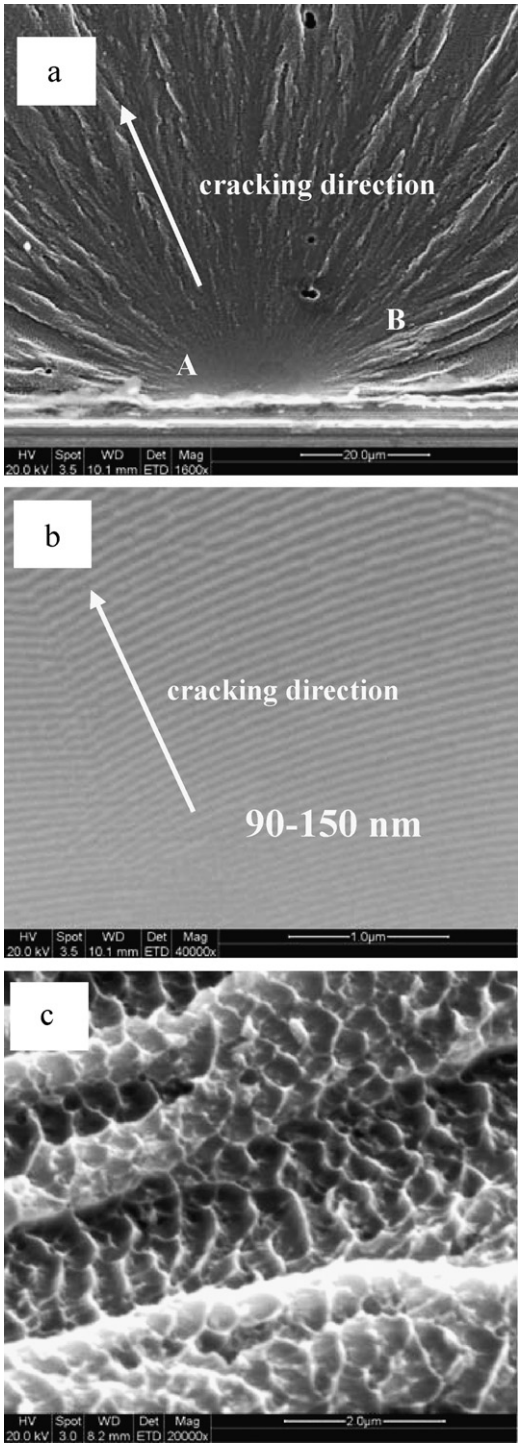

Fig. 4. The SEM images of the three-point bending fracture morphology of S20 alloy (a) and the higher magnification of crack initiation (b) and instantaneous fracture zone (c), respectively.

dimensional structure of the grain after the instantaneous fracture at the overload region, as shown in Fig. 6(c).

The question then arises as to why the S16 alloy with more dendrite phase holds lower fracture toughness as compared to S18 alloy. To clarify this enquiry, the detailed study of microstructure of the two alloys was carried out using TEM. Fig. 7(a) shows the TEM bright field image of S18 alloy, revealing clearly a mixing structure containing dendrites and amorphous phase. The selected area diffraction (SAD) pattern of one dendrite as shown

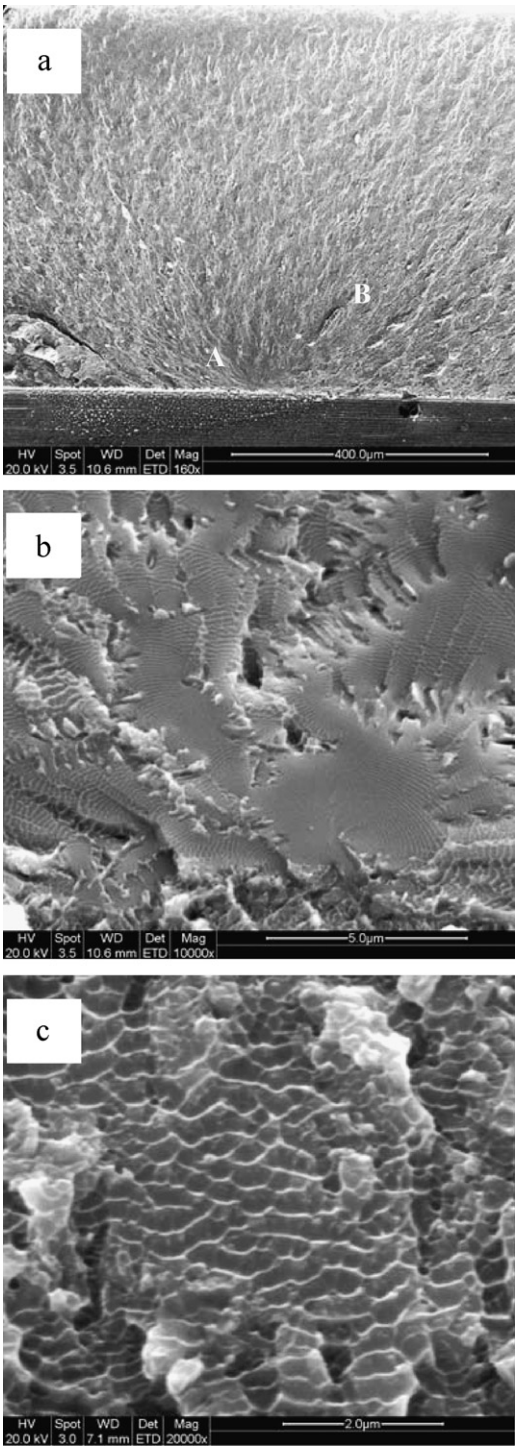

Fig. 5. The SEM micrographs for the bending fracture morphology of S18 alloy (a) and the higher magnification of crack initiation (b) and instantaneous fracture zone (c), respectively.

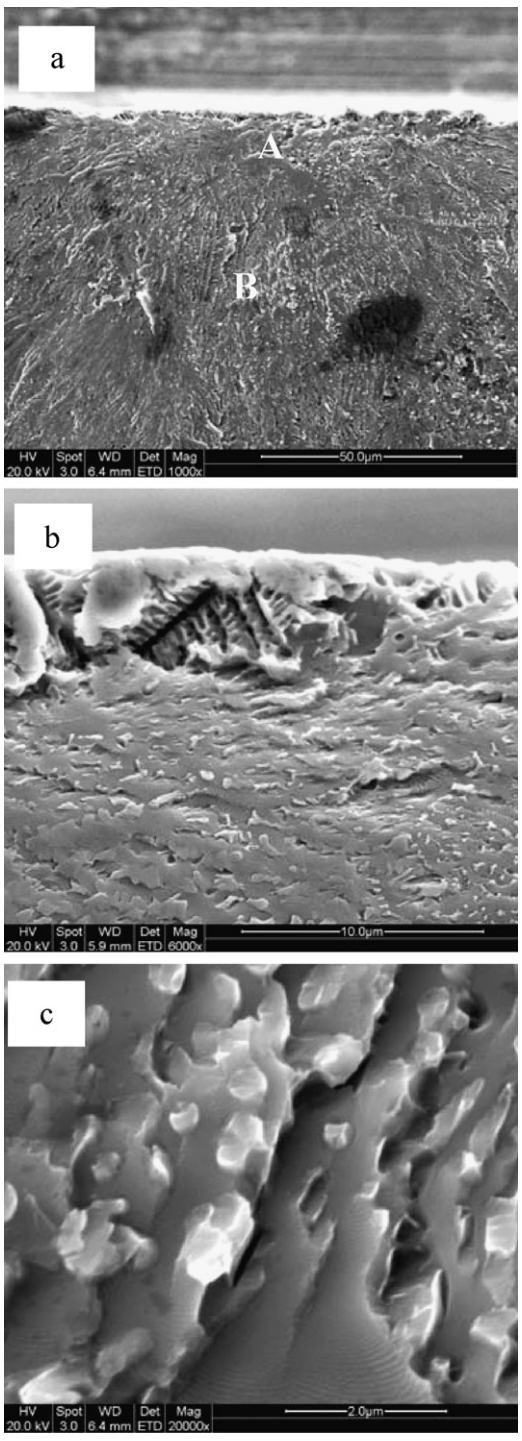

Fig. 6. The SEM micrographs for the bending fracture morphology of S16 alloy (a) and the higher magnification of crack initiation (b) and instantaneous fracture zone (c), respectively.

in Fig. 7(b) exhibits obviously a BCC structure with the lattice constant of 2.87 Å, corresponding to α-Fe. It also exhibits a composite structure for the S16 alloy as shown in Fig. 7(c). However, the SAD pattern of the dendrite displays two sets of diffraction spots as shown in Fig. 7(d). Fig. 7(e) and (f) show the TEM dark field image taken from one diffraction spot from each SAD pattern, respectively. It was revealed that the strong pattern is from the diffractions of α-Fe as the same as S18 alloy, while the weak SAD pattern corresponds to the diffractions from impurity phase of FeMoP compound in S16 alloy. The FeMoP compound is known as a very brittle phase, whose precipitation could account for the deterioration of the fracture toughness of S16 alloy even though it contains more ductile dendrite phase [19]. This result is similar to structural relaxation during annealing of the BMG below T_g or partial crystallization at higher temperatures, which appeared some phase embrittlement tendency and leads to a decrease in toughness [20,21].

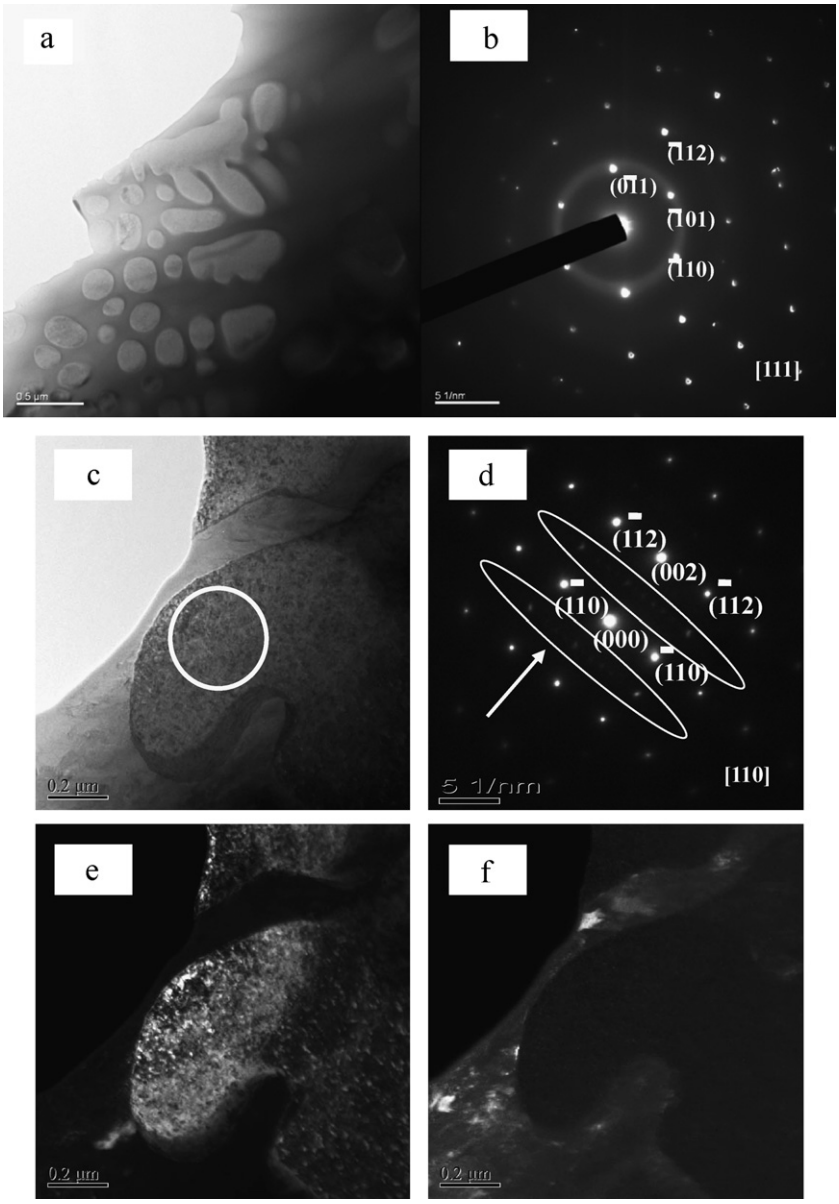

Fig. 7. (a) TEM bright field image of the dendrite phase of S18 alloy and (b) SAED pattern of the dendritic phase taken along [1 1 1] zone axis; (c) TEM bright field image of the dendrite phase of S16 alloy and (d) the SAED pattern of the dendritic phase taken along [1 1 0] zone axis; (e) and (f) show the TEM dark field according to the two sets of diffraction spots shown in (d), respectively.

4. Conclusions

This paper reported on the notch fracture toughness of the three Fe-based alloys including $Fe_{75}Mo_5P_{10}C_{8.3}B_{1.7}$ monolithic BMG, and $Fe_{77}Mo_5P_9C_{7.5}B_{1.5}$ and $Fe_{79}Mo_5P_8C_{6.7}B_{1.3}$ BMG matrix composites. The monolithic BMG exhibits a pretty good toughness of 27 MPa $m^{1/2}$ owing to its low glass transition temperature. The toughness could be significantly enhanced up to 40 MPa $m^{1/2}$ in $Fe_{77}Mo_5P_9C_{7.5}B_{1.5}$ composite due to the precipitation of pure α-Fe dendrite, which prevents the rapid unstable operation of the shear band and promote the crack bifurcation. However, the toughness is deteriorated for $Fe_{79}Mo_5P_8C_{6.7}B_{1.3}$ BMG matrix composite with more α-Fe dendrites because of the precipitation of a small amount of brittle phase of FeMoP compounds apart from α-Fe. It is proposed that the intrinsic properties of precipitation phase may play more important role in the fracture toughness rather than the formation of dendrite phase.

Acknowledgements

This work is financially supported by National Nature Science Foundation of China (Grant No. 50871042) and the National Fundamental Research Program of China (Grant No. 2007CB613908). This work was partially supported by the Research Grants Council of The Hong Kong Special Administration Region (Project No. PolyU5112/07E) and the internal funding from ISE department, the Hong Kong Polytechnic University. Authors are grateful to the Analytical and Testing Center, HUST for technical assistances.

References

[1] C.A. Schuh, T.C. Hufnagel, U. Ramamurty, Acta Mater. 55 (2007) 4067.
[2] K. Mondal, K. Hono, Mater. Trans. JIM 50 (2009) 152.
[3] Z. Han, W.F. Wu, Y. Li, Y.J. Wei, H.J. Gao, Acta Mater. 57 (2009) 1367.
[4] P. Lowhaphandu, J.J. Lewandowski, Scr. Mater. 38 (1998) 1811.
[5] P. Jia, Z.D. Zhu, E. Ma, J. Xu, Scr. Mater. 61 (2009) 137.

[6] X.J. Gu, S.J. Poon, G.J. Shiflet, J.J. Lewandowski, Acta Mater. 58 (2010) 1708.
[7] J. Xu, U. Ramamurty, E. Ma, JOM 64 (2010) 10.
[8] A. Inoue, B.L. Shen, A.R. Yavari, A.L. Greer, J. Mater. Res. 18 (2003) 1487.
[9] S.F. Guo, L. Liu, X. Lin, J. Alloys Compd. 478 (2009) 226.
[10] P.A. Hess, S.J. Poon, G.J. Shiflet, R.H. Dauskardt, J. Mater. Res. 20 (2005) 783.
[11] J.J. Lewandowski, X.J. Gu, A. Shamimi Nouri, S.J. Poon, G.J. Shiflet, Appl. Phys. Lett. 92 (2008) 091918.
[12] S.F. Guo, L. Liu, N. Li, Y. Li, Scr. Mater. 62 (2010) 329.
[13] Y. Murakami, Stress Intensity Factors Handbook, vol. 2, Pergamon, Oxford, United Kingdom, 1987, p. 666.
[14] D.C. Hofmann, Ph. D. Thesis, California Institute of Technology, California, 2009.
[15] M.D. Demetriou, G. Kaltenboeck, J.Y. Suh, G. Garrett, M. Floyd, C. Crewdson, D.C. Hofmann, H. Kozachkov, A. Wiest, J.P. Schramm, W.L. Johnson, Appl. Phys. Lett. 95 (2009) 041907.
[16] X.K. Xi, D.Q. Zhao, M.X. Pan, W.H. Wang, Y. Wu, J.J. Lewandowski, Phys. Rev. Lett. 94 (2005) 125510.
[17] G. Wang, Y.T. Wang, Y.H. Liu, M.X. Pan, D.Q. Zhao, W.H. Wang, Appl. Phys. Lett. 89 (2006) 121909.
[18] G. Wang, D.Q. Zhao, H.Y. Bai, M.X. Pan, A.L. Xia, B.S. Han, X.K. Xi, Y. Wu, W.H. Wang, Phys. Rev. Lett. 98 (2007) 235501.
[19] C.H. Shek, G.M. Lin, K.L. Lee, J.K.L. Lai, J. Non-Crystalline Solids 224 (1998) 244.
[20] N. Nagendra, U. Ramamurty, T.T. Goh, Y. Li, Acta Mater. 48 (2010) 2603.
[21] J. Basu, N. Nagendra, Y. Li, U. Ramamurty, Philos. Mag. 83 (2003) 1747.